Journal of Magnetic Resonance **154,** 298–302 (2002)
doi:10.1006/jmre.2001.2482, available online at http://www.idealibrary.com on IDEAL®

An Open Magnet Utilizing Ferro-Refraction Current Magnification

Yuly Pulyer* and Mirko I. Hrovat†

**Department of Radiology, Brigham and Women's Hospital, 75 Francis Street, Boston, Massachusetts 02115; and †Mirtech, Inc., 452 Ash Street, Brockton, Massachusetts 02301*

Received August 13, 2001; revised November 9, 2001; published online January 16, 2002

Ferro-refraction is the field magnification that is obtained when a current segment is near a high magnetic permeable boundary. It is shown that ferro-refraction may be used in the design of magnets for NMR or MRI to increase the efficiency of these magnets. The field may be modeled analytically with the Biot–Savart law and the inclusion of mirror image currents. Ferro-refraction is particularly useful in the design of monohedral magnets, magnets producing a remote homogeneous region which have the magnetic sources arranged to one side. These magnets have also been called planar magnets. Two designs for a monohedral magnet which produce good agreement between experimental and analytic results are presented.

Key Words: **ferro-refraction; magnet; monohedral; planar; magnetic refraction; mirror image.**

INTRODUCTION

The open MRI (magnetic resonance imaging) magnet has been established for several recent years as a powerful imaging tool for imaging guided medical procedures (*1*, *2*). To date, most practical designs consist of standard magnet designs that are engineered to provide more access to the central magnetic region. Thus, split solenoids or C-magnets have often been employed. A recent classification scheme has termed these magnets as bihedral since the magnetic sources are arranged around two sides of the sample or patient (*3*). On the other hand, monohedral designs, which have magnetic sources arranged to one side, are truly "open" in that the structure of the magnet does not impede access to the sample or patient. This "*openness*" may revolutionize surgery by providing all MR techniques to the operating room. The first of this type of magnet was used in an industrial application and provided an external radial field (*4*). Other monohedral designs have been proposed (*5–11*). Clearly the primary advantage of monohedral magnets over bihedral magnets is their openness. However, bihedral magnets benefit from a well-developed analytic design theory which has led to high field and high homogeneous designs that are in current use. This development is in its infancy for monohedral magnets. Consequently, current monohedral magnets do not generate high fields or high homogeneity. With further development it is expected that homogeneity should be comparable to current bihedral magnets. The ability to generate high fields is related to magnet efficiency. At first it may seem that monohedral magnets are less efficient then their open bihedral counterparts; however, we have demonstrated, in principle, that monohedral magnets are comparable in efficiency (*3*). The efficiency may be further improved through the use of ferro-refraction.

Ferro-refraction refers to the field magnification that may be obtained when a current segment is near a high magnetic permeability (μ) boundary. Refraction occurs at any boundary surface between two materials of different permeability. At the surface, the normal components of the magnetic induction (B) are equal, while the tangential components of the magnetic field (H) are equal (*12*). This is illustrated in Fig. 1 where it is seen that the field is refracted according to the refraction equation given by

$$\mu_1 \operatorname{ctg} \theta_1 = \mu_2 \operatorname{ctg} \theta_2. \qquad [1]$$

If $\mu_2 \gg \mu_1$ then $\theta_1 \sim 0^\circ, \theta_2 \sim 90^\circ$. Thus refraction at a ferro-magnetic boundary (ferro-refraction) leads to orthogonal boundary conditions. The consequence of this is best illustrated by some simple geometric examples. In Fig. 2, three geometries are shown with a single current wire placed in the vicinity of a ferro-magnetic boundary ($\mu = \infty$). The method of images (*12*), which utilizes the above orthogonality relationship at the interface, allows for a simple interpretation. In all three cases of Fig. 2, the resulting field may be calculated as if there are virtual mirror image currents placed symmetrically with respect to the boundaries. This distribution reproduces the orthogonal boundary condition. Unlike eddy currents, the mirror image currents are parallel with the actual current and thus substantially increase the field strength. In particular, Fig. 2C illustrates that orthogonal ferro-magnetic boundaries produce three virtual currents, and hence provides a maximum fourfold magnification factor.

RESULTS

We have investigated the possible use of the ferro-refraction concept for magnet designs with an experimental configuration shown in Fig. 3. This design generates a remote saddle point for

1090-7807/02 $35.00

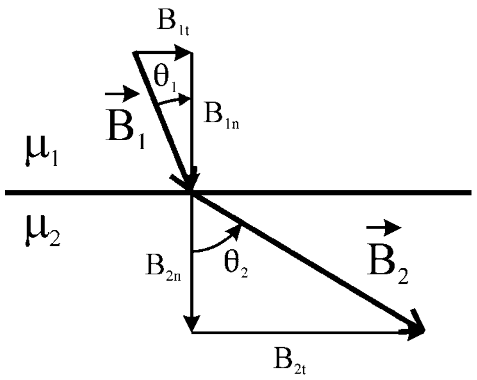

FIG. 1. Refraction of the magnetic induction field at an interface. $B_{1n} = B_{2n}$, $B_{1t}/\mu_1 = B_{2t}/\mu_2$.

the B_z component of the field and is an example of an open MRI magnet (*13*). Without a ferromagnetic core material, the current loops do not generate any significant magnetic field, since the field generated by the far side of the loop will cancel the field from the near side. However, if even a few high μ transformer laminations are inserted inside of the two current loops, then there will be an appreciable external field. B_z along x is shown in Fig. 3 with the field maximum along x indicated by B_m. Measurements of B_z, at a fixed distance corresponding to the location of B_m, as a function of the number of laminations, n, are shown in Fig. 4. Clearly, the laminations shield the magnetic field contribution from the far side of the current loops. The functional dependence of B_z upon n may be quantified using an equivalent magnetic circuit model. Referring to Fig. 5, the electromotive force is provided by the two current loops. The magnetic field flux in air on each side of the magnet is given by Φ_A with the reluctance represented by R_A and the flux in the magnetic core is given by Φ_C with the reluctance represented by R_C. This gives the circuit equation

$$2IN = \Phi_C R_C + \Phi_A R_A, \qquad [2]$$

where IN is the ampere turns of each current loop. The reluctance of the core is given approximately by $R_C = lc/\mu_o \mu_c l_m t_1 n \equiv \alpha/n$, where the thickness of the lamination is given by t_1 and the relative permeability of the core is given by μ_c. Assuming that Φ_A is proportional to B_z ($\Phi_A \equiv k B_z$), and noting that $\Phi_C = 2\Phi_A$, gives

$$B_z = \frac{2IN}{kR_A}\frac{n}{n + 2\alpha/R_A}. \qquad [3]$$

The form of Eq. [3] agrees well with the data in Fig. 4, with $2IN/kR_A = 61.7$ G and $2\alpha/R_A = 1.03$.

B_z may be also be expressed utilizing the Biot–Savart law. The magnetic field along x at $y = z = 0$ for two current segments (current $= IN$) of length l_m in free space is given by

$$B_z(x) = \frac{\mu_o IN}{\pi}\frac{x l_m/2}{(h^2 + x^2)\sqrt{h^2 + x^2 + (l_m/2)^2}}. \qquad [4]$$

The field strength increases with increasing l_m and thus for a

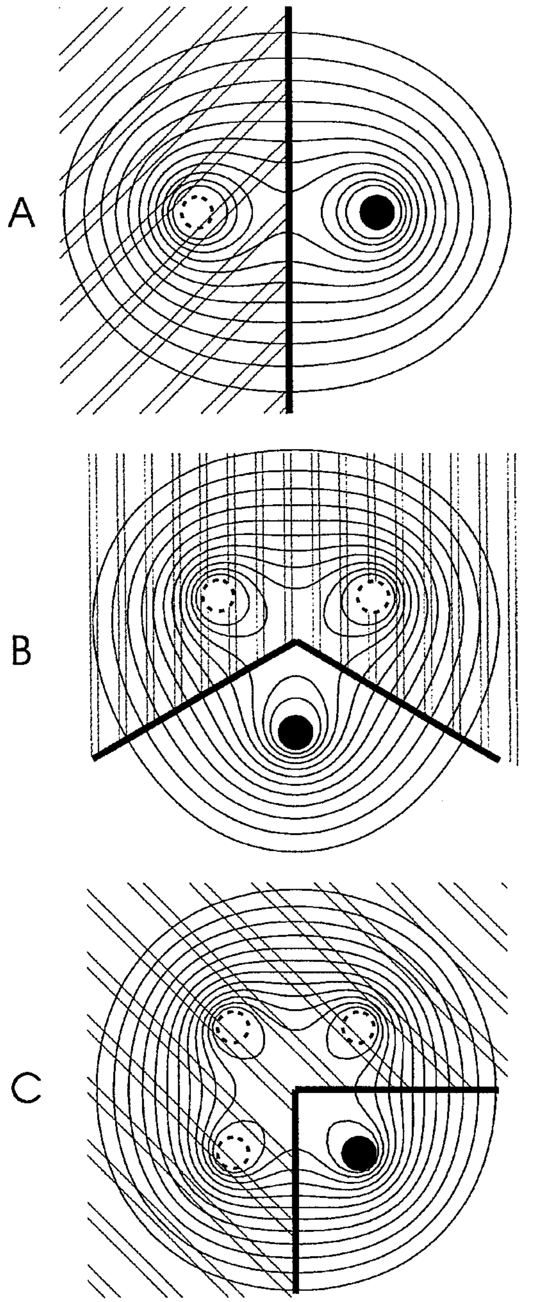

FIG. 2. Field magnification provided by ferro-refraction. The magnetic field lines generated by a single current wire (solid circle) in the presence of a high μ boundary is equivalent to the magnetic field generated with additional mirror image currents (dashed circle). (A) Planar ferro-refraction. (B) Tri-ferro-refraction. (C) Quadru-ferro-refraction.

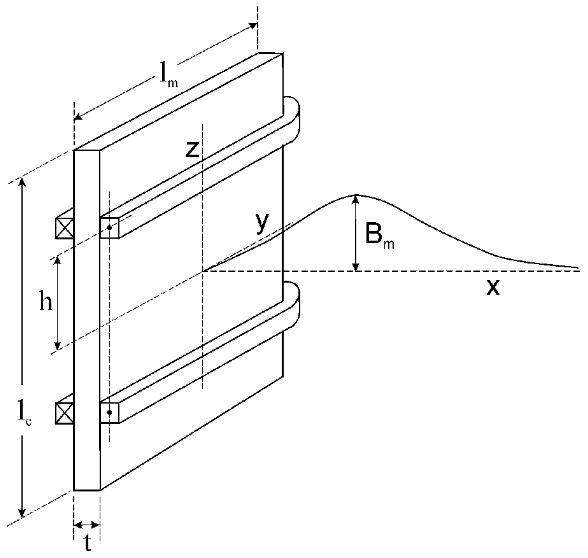

FIG. 3. Two current loops wrapped around a ferromagnetic core. The core consists of M6 transformer steel laminations of thickness 0.3 mm and the number of laminations was varied from 0 to 15. Additional parameters are $l_c = 12$ cm; $l_m = 12$ cm; $h = 2.25$ cm; $t = 2$ cm; $N = 100$ turns; $I = 5$ A.

given spacing, h, it is desirable to have $l_m \gtrsim 2h$. The maximum in this function is found by setting the derivative of B_z with respect to x to zero, to give

$$x_{\max}^2 = \frac{1}{4}[h^2 + (l_m/2)^2]\left(\sqrt{1 + \frac{8\,h^2}{h^2 + (l_m/2)^2}} - 1\right). \qquad [5]$$

By $\nabla \cdot B = 0$, $x_{\max}$ must also be a saddle point. An important feature of the above equation is that the saddle point position is

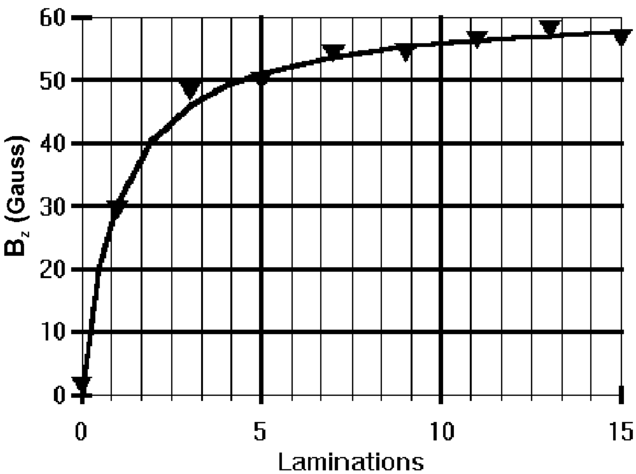

FIG. 4. $B_z(x = 2$ cm) as a function of the number of laminations. Measurements were made with a Hall probe and a Bell 9000 Gaussmeter. The solid line is a calculated fit to the data.

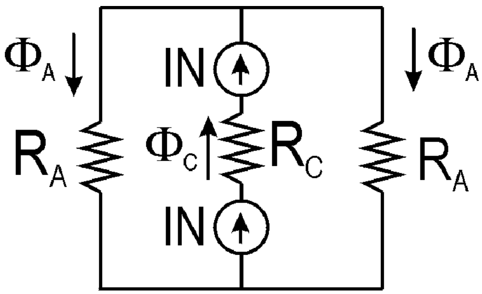

FIG. 5. Equivalent magnetic circuit for Fig. 3.

dependent upon the spacing of the current wires, h. Therefore, the remoteness of the field may be controlled by the spacing. The dependence of Eq. [5] upon l_m is less significant, since $x_{\max}$ is bounded between $h/\sqrt{2}$ and h as $l_m \to 0$ to ∞. Utilizing the parameters above, $B_m = B_z(x_{\max})$ is calculated to be 39.4 G. This value may be doubled to reflect the contribution of image currents. A more accurate calculation taking into account the distance of the center of the wire from the laminations (0.5 cm) along with inclusion of the mirror image currents gives a value of 76 G. This compares favorably with the experimental value of 61.7 G measured. The maximum in $B_z(x)$ occurred at 2 cm which is in agreement with the calculated value of 2.05 cm.

This example concisely demonstrates two main advantages provided by high μ materials. One advantage derives from the magnetic shielding of the return currents, which significantly improves efficiency. Normally, the main method for reducing the magnetic field contribution is to lengthen the return path with a concomitant increase in resistance and inductance. Interestingly, magnetic shielding permits the field to be modeled in terms of current segments (as in Eq. [4]) as opposed to current loops. The second advantage provided by high μ materials is the effect of field magnification. This effect may be modeled as arising from mirror image currents. Thus, the contribution of the ferromagnetic core may be accounted for by the simpler introduction of mirror image currents.

Further magnification by ferro-refraction is suggested by the example in Fig. 2C. Two orthogonal ferromagnetic boundaries with high permeability will produce three mirror image currents for each current wire. This effect we have termed quadru-ferro-refraction (QFR). To confirm the QFR effect, we have built a laboratory prototype which has a central planar core plate and two main additional orthogonal plates on top and bottom made from the same transformer laminations described earlier. The magnet with dimensions is shown in Fig. 6. The field was mapped by a 3D coordinate table to which was attached a Hall probe. Figure 7 shows B_m as a function of the top and bottom plate lenghts, l_h, illustrating that finite lengths for these plates is practical. Note the increase in field strength, which is suggestive of contribution from additional mirror image currents as predicted for a QFR effect. The field profile for the QFR

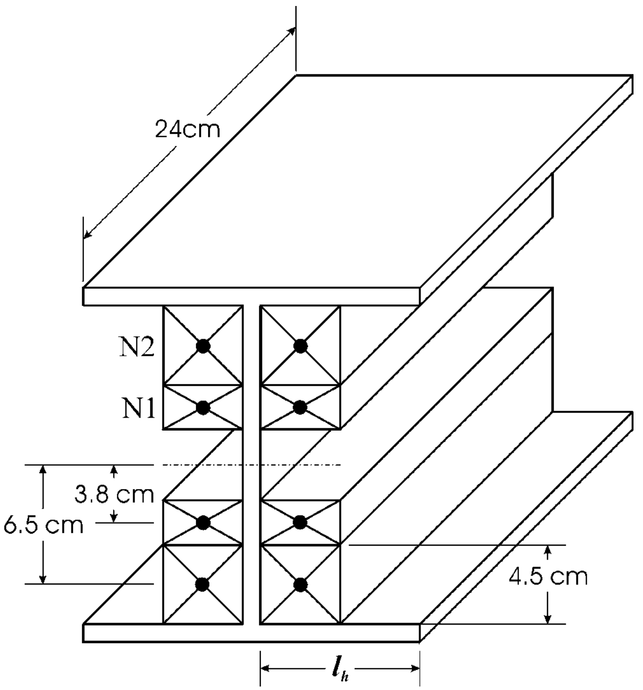

FIG. 6. QFR magnet. Two main coil pairs, N_1 and N_2, are used to produce the background field, B_0, with the following parameters: Core thickness = 8 mm; N_1, $N_2 = 100$, 547 turns of 18 AWG solid copper wire; current = 3A with air cooling; warm-up time, 30 min.

magnet was measured along x as shown in Fig. 8. Notice that a maximum is exhibited at about $x = 7.5$ cm. Coarse adjustment of the location of the maximum and homogeneity is affected by the vertical positions of the coils as well as relative current strengths. In principle further refinement of the homogeneity could be provided by additional horizontal current segments whose current and position are varied (shim segments). The N_1 coil is an example of such a segment. The solid line in Fig. 8 is a computation of the field profile based on Eq. [4]

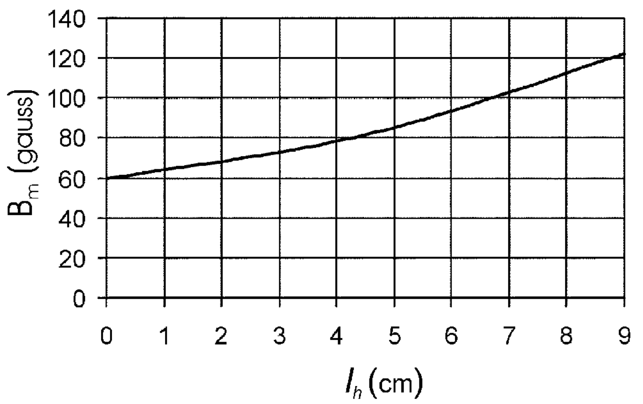

FIG. 7. Experimental field strength dependence of the QFR magnet on the length of the horizontal plate, l_h.

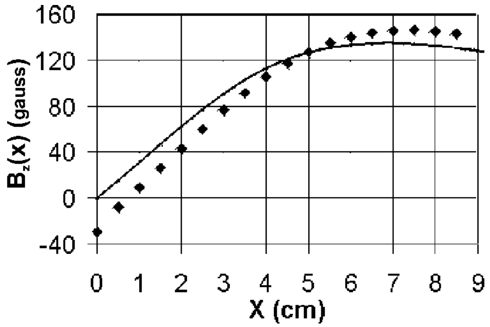

FIG. 8. Measured field profile (◆) along x of the QFR magnet, $l_h = 9$ cm. The solid line is computed based upon Eq. [4] and the inclusion of three mirror image currents.

taking into account all three image currents for each coil. The agreement is good. Without the inclusion of mirror image currents, the calculated maximum is 54 G. This should be compared with the experimental maximum value of 146 G, which is an increase of 170%. From theoretical calculations, the N_1 coil benefits by an increase of 91% from ferro-refraction while the N_2 coil increases by 172% and contributes 80% of the total field. Thus the N_1 coil has significant contributions from only one mirror image current while the N_2 coil has significant contributions from effectively two mirror image currents. This is less than the expected value of three since the thickness of the coils moves the centers of the mirror image currents further away.

CONCLUSION

It has been demonstrated that a magnet utilizing ferro-refraction can generate a remote saddle point. This is a minimal requirement for any "open" MRI magnet, if such a magnet is to be homogeneous. The remoteness of the field is controlled by the spacing between the current elements. This flexibility is important for the design of a homogenous region which is not adjacent to the magnetic sources. Even though ferro-refraction has been applied in this paper for a monohedral magnet, it should be evident that two monohedral magnets may always be combined to create a more traditional bihedral design. Thus the principles elucidated here are applicable to designs of many types of magnets. The primary benefit of ferro-refraction is to improve the efficiency of electromagnet systems. A secondary feature of ferro-refraction is that the effect of the ferromagnetic boundary may be analytically simulated through the inclusion of image currents. This analytic simplification may prove useful in the design of magnets.

ACKNOWLEDGMENT

We thank the Department of Radiology and Mirtech, Inc., for their financial support.

REFERENCES

1. F. A. Jolesz, Image-guided procedures and the operating room of the future, *Radiology* **204,** 601–612 (1997).
2. F. A. Jolesz, Interventional and interoperative MRI: A general overview of the field, *J. Magn. Reson. Imaging* **8,** 3–6 (1998).
3. Y. M. Pulyer and M. I. Hrovat, Generation of remote homogeneous magnetic fields, *IEEE Trans. Magn.*, to appear.
4. R. K. Cooper and J. A. Jackson, Remote (inside-out) NMR. I. Remote production of a region of homogeneous magnetic field, *J. Magn. Reson.* **41,** 400–405 (1980).
5. A. R. Rath, S. B. W. Roeder, and E. Fukushima, Opposed coil magnet calculation for large sample and unilateral nuclear magnetic resonance, *Rev. Sci. Instrum.* **56**(3), 402–410 (1985).
6. I. L. McDougall and J. M. Bird, “Magnet Assembly Having a Plurality of Nested Coaxial Coils,” U.S. Patent 4701736 (Oct. 20, 1987).
7. B. Dorri and E. T. Laskaris, “Pancake MRI Magnet with Modified Imaging Volume,” U.S. Patent 5428292 (June 27, 1995).
8. E. T. Laskaris and M. D. Ogle, “Planar Superconducting MRI Magnet,” U.S. Patent 5677630 (Oct. 14, 1997).
9. Y. M. Pulyer, “Planar Open Magnet for MRI Systems,” U.S. Patent 5477960 (Apr. 28, 1998).
10. Y. M. Pulyer, “Planar Open Solenoidal Magnet MRI System,” U.S. Patent 5914600 (June 22, 1999).
11. Y. M. Pulyer, “Planar Open Magnet MRI System Having Active Target Field Shimming,” U.S. Patent 6002255 (Dec. 14, 1999).
12. W. R. Smythe, “Static and Dynamic Electricity,” pp. 306–307, 311–312 (ferro-refraction). 3rd ed., Hemisphere, New York (1989).
13. Y. M. Pulyer, “Planar Open MRI Magnet Based on Ferro-Refraction Field Magnification Concept,” U.S. Patent Pending 09-746967 (Dec. 22, 2000).